Virologica Sinica 39 (2024) 574–586

Contents lists available at ScienceDirect

Virologica Sinica

journal homepage: www.keaipublishing.com/en/journals/virologica-sinica
www.virosin.org

Research Article

NSUN2 mediates distinct pathways to regulate enterovirus 71 replication

Lishi Liu [a,b,1], Zhen Chen [a,1], Kui Zhang [a,b], Haojie Hao [a], Li Ma [a,b], Haizhou Liu [a], Baocheng Yu [a,b], Shuang Ding [a], Xueyan Zhang [a], Miao Zhu [a,b], Xiang Guo [a,b], Yi Liu [c], Haibin Liu [a], Fang Huang [c,*], Ke Peng [a,c,*], Wuxiang Guan [a,c,*]

[a] Center for Emerging Infectious Diseases, Wuhan Institute of Virology, Center for Biosafety Mega-Science, Chinese Academy of Sciences, Wuhan, Hubei, 430071, China
[b] University of Chinese Academy of Sciences, Beijing, 100049, China
[c] Hubei Jiangxia Laboratory, Wuhan, Hubei, 430200, China

ARTICLE INFO

Keywords:
NSUN2
5-methylcytosine
Enterovirus 71
Ubiquitination
Pathogenicity

ABSTRACT

Increasing evidences suggest that the methyltransferase NSUN2 catalyzes 5-methylcytosine (m5C) modifications on viral RNAs, which are essential for the replication of various viruses. Despite the function of m5C deposition is well characterized, other potential roles of NSUN2 in regulating viral replication remain largely unknown. In this study, the m5C modified residues catalyzed by NSUN2 on enterovirus 71 (EV71) RNAs were mapped. NSUN2, along with m5C modifications, played multiple roles during the EV71 life cycle. Functional m5C modified nucleotides increased the translational efficiency and stability of EV71 RNAs. Additionally, NSUN2 was found to target the viral protein VP1 for binding and promote its stability by inhibiting the ubiquitination. Furthermore, both viral replication and pathogenicity in mice were largely attenuated when functional m5C residues were mutated. Taken together, this study characterizes distinct pathways mediated by NSUN2 in regulating EV71 replication, and highlights the importance of its catalyzed m5C modifications on EV71 RNAs for the viral replication and pathogenicity.

1. Introduction

RNA modifications are characterized by the deposition of chemical moieties (Song et al., 2021; Wiener and Schwartz, 2021; Deng et al., 2022), which have been demonstrated to play crucial roles in gene expression (Wu et al., 2013). Three types of enzymes, namely "writers" to deposit the chemical moiety on RNAs, "erasers" to remove such chemical modifications, and "readers" to interpret the indicated RNA modifications, determine the biogenesis and function of RNA modifications (Shi et al., 2019; Wang et al., 2020). To date, more than 170 different RNA modifications have been discovered, and have been reported to be involved in various cellular events (Dawson and Kouzarides, 2012; Roundtree et al., 2017). Approximately ten distinct modifications have been characterized in mRNAs, including N6-methyladenosine (m6A), 5-methylcytosine (m5C), pseudouridine (Ψ), N7-methylguanosine (m7G), 2′-*O*-Methylation (Nm), and N4-acetylcytidine (ac4C) (Meyer, 2019). It has been well documented that viral replication strictly relies on the host cell machinery (Majumder and Morales, 2021; Srinivas et al., 2021). Similar to host RNAs, viral RNA molecules are also highly modified during viral replication (Zhao et al., 2020; Li et al., 2021). The modification of viral RNAs of human immunodeficiency virus 1 (HIV-1) (Kennedy et al., 2016; Lichinchi et al., 2016; Courtney et al., 2019b; Tsai et al., 2020) and murine leukemia virus (MLV) (Courtney et al., 2019a; Eckwahl et al., 2020) is associated with markedly higher levels of m6A, m5C, Nm, and ac4C residues than those on cellular mRNAs. These findings suggest that these modifications contribute to one or more steps in the viral replication cycle.

m5C modification is defined as methylation at the 5th position of the cytosine pyrimidine ring at a specific site (Lv et al., 2021). NOP2/SUN (NSUN) family proteins, as well as the DNA methyltransferase (DNMT) homologue DNMT2, were identified as the predominant "writers" that catalyze m5C modifications on RNAs (Reid et al., 1999). Whereas the "erasers" remain elusive, both ALYREF and YBX1 are characterized as the "readers" of m5C modifications (Chen et al., 2019; Yang et al., 2019). The mRNA export adaptor ALYREF exclusively recognizes m5C and promotes the nuclear export and translation of m5C-modified RNA (Yang et al., 2017), and YBX1 is characterized as an m5C-binding protein that regulates m5C-modified maternal mRNA stability (Yang et al., 2019; Song et al., 2021).

* Corresponding authors.
E-mail addresses: guanwx@wh.iov.cn (W. Guan), pengke@wh.iov.cn (K. Peng), huangf@wh.iov.cn (F. Huang).
[1] Lishi Liu and Zhen Chen contributed equally to this work.

https://doi.org/10.1016/j.virs.2024.05.002
Received 3 March 2024; Accepted 3 April 2024
Available online 18 May 2024

The non-enveloped virus enterovirus 71 (EV71) causes global outbreaks of hand, foot, and mouth disease, mostly in children (Chen et al., 2015). The EV71 genome is a single-stranded, positive-stranded RNA consisting of a 5′-untranslated region (5′ UTR), an open reading frame, a 3′ UTR, and a poly-A tail with a variable length at the 3′ end (Xiao et al., 2019). Cellular RNA-binding proteins bind to the 5′ UTR of EV71 RNA to produce viral polyproteins. The internal ribosome entry site (IRES) motif is located in the 5′ UTR of EV71 and is essential for the initiation of translation (Lin et al., 2008; Sweeney et al., 2014). The entire EV71 coding region consists of three segments as follows: P1, encoding four structural proteins, VP1, VP2, VP3, and VP4; P2 and P3 encoding another seven non-structural proteins, 2A, 2B, 2C, 3A, 3B, 3C, and 3D respectively (Cardosa et al., 2003; Pathinayake et al., 2015). Recent studies showed that m6A and ac4C modifications on EV71 RNAs, along with their indicated "writers" METTL3 and NAT10, promote viral replication (Hao et al., 2019, 2022). Moreover, host epitranscriptomic landscapes are altered by viral infections, and these global changes have been shown to affect viral replication. However, whether EV71 RNAs harbor m5C modifications and how NSUN2 and m5C modifications affect viral replication remain unknown.

Recent reports have revealed that NSUN2 is the methyltransferase that catalyzes the m5C modifications of HIV-1 (Courtney et al., 2019b), MLV (Eckwahl et al., 2020) and HBV (Feng et al., 2023; Ding et al., 2024). Similar to that of host mRNAs, the m5C modifications of these viral transcripts are pivotal for viral replication. The loss of m5C modifications via the depletion of NSUN2 specifically reduces the translation efficiency of HIV-1 and HBV transcripts and cellular mRNAs, which are normally m5C-modified. Meanwhile, the dominant negative mutant NSUN2/C321A, which will not be able to catalyze the m5C modification properly (Hussain et al., 2013), has been proven to reverse such WT NSUN2-mediated effects on these viruses. Further, the NSUN2 deficiency leads to disorders in the alternative splicing of viral RNAs (Courtney et al., 2019b). Nevertheless, how m5C modifications regulate viral replication and whether NSUN2 is capable of directly regulating viral replication are still largely unknown.

In this study, we verified that EV71 RNA contains m5C modification by UPLC-MS/MS, dot blot and MeRIP-qPCR, etc. The distribution of m5C modified residues on EV71 RNAs were mapped and identified by nanopore-based direct RNA sequencing. Importantly, the functional m5C sites were involved in viral replication, protein translation and pathogenicity in mice. Beyond the enzymatic activities of NSUN2, the interactions between NSUN2 and viral protein VP1 were revealed by co-IP assays, which led to inhibit the K48-linked ubiquitination of VP1 and promote its stability. Overall, we characterized distinct pathways mediated by NSUN2 to regulate enterovirus 71 replication, which not just broad the understanding of crosstalk between RNA modification and viral replication, but also provides potential targets for the drug development against EV71 infection.

2. Materials and methods

2.1. Plasmids, antibodies and reagents

Plasmids: The pcDNA3.0-NSUN2 was constructed by inserting the coding sequence (CDS) of NSUN2 into pcDNA3.0 vector (Invitrogen, Carlsbad, CA, USA). pFlag-NSUN2, pFlag-DNMT2, pFlag-ALYREF and pFlag-VP1 from EV71 XF strain, were constructed into pXJ40-Flag vector (Sigma-Aldrich, St. Louis, MO, USA). The m5C modified residues mutated EV71 infectious clones were constructed by substituting C to G (nt 2637 and nt 7009) or to A (nt 1460), and EV71 infectious clone (Mut-584) was constructed by both substituting C to G at nt 584 and G to C at nt 621, based on the WT EV71 infectious clone (provided by Prof. Bo Zhang's laboratory). Two chimeric reporter plasmids were constructed by inserting the EV71 WT or m5C mutant (Mut-584) 5′UTR into the location between the cytomegalovirus (CMV) promoter and the CDS fragment of enhanced green fluorescent protein (eGFP) in pEGFP-N1 (Clontech, Mountain view, CA, USA) or firefly luciferase in pGL3-basic-vector. Plasmids of EV71 WT- and m5C mutant-3D mut were constructed by deleting the first nucleotide of the 3D coding region based on above infectious EV71 clones.

Antibodies (Abs) used for Western blot (WB) and immunofluorescence confocal microscopy in this study: anti-GAPDH (60004-1-lg, Proteintech, Rosemont, IL, USA), anti-beta-Actin (sc-47778, Santa Cruz Biotechnology, Dallas, TX, USA), anti-NSUN2 (66580-1-Ig, Proteintech), anti-DNMT2 (NB200-587, NOVUS, Centennial, CO, USA), anti-ALYREF (H00010189, NOVUS), anti-YBX1 (20339-1-AP, Proteintech), anti-Flag (F1804 MG, Sigma-Aldrich), anti-HA (66006-1-Ig, Proteintech), anti-VP1 (GTX633390, GeneTex, Irvine, CA, USA), anti-m5C (ab10805, Abcam), mouse (B900620, Proteintech) and rabbit control IgG (30000-0-AP, Proteintech), ECL mouse or rabbit IgG HRP-linked whole Ab (Anti-Gene Biotech GmbH, Stuttgart, Germany) and Alexa Fluor 488/568 goat anti-mouse/rabbit IgG Abs (Invitrogen).

Reagents: Cycloheximide (CHX) was purchased from Sigma-Aldrich, and Hoechst 33258 were purchased from Invitrogen. *In vitro* transcription experiment was completed by using MEGAscript™ T7 transcription kit (AM1333, Thermo Fisher, Gaithersburg, MD, USA).

2.2. Cell culture, cell manipulation, virus preparation

Vero (CCL-81, American Type Culture Collection (ATCC), Manassas, VA, USA), HEK293T (CRL-11268, ATCC), and RD (CCL-136, ATCC) cells were cultured in Dulbecco's modified Eagle's medium (DMEM) (C11995500BT, Thermo Fisher) supplemented with 10% fetal bovine serum (FBS) (Gibco) at 37 °C and 5% CO_2. Plasmid transfection was performed using Lipofectamine 2000 (Life Technology) according to the manufacturer's instructions.

EV71 (strain XF) was obtained from the Microorganisms & Viruses Culture Collection Center (MVCCC), Wuhan Institute of Virology (WIV), Chinese Academy of Sciences (CAS). Viruses were amplified in Vero cells, and the indicated 50% tissue culture infectious doses ($TCID_{50}$) were titrated in Vero cells. EV71 infection was conducted with MOI 0.1 for Vero and RD cells. To produce WT or mutant EV71 viruses based on the indicated infectious clone, *In vitro* EV71 RNAs were transcribed from linearized plasmids of WT or mutant EV71 infectious clone using MEGAscript® T7 Kit (Ambion, Austin, TX, USA) according to the manufacturer's instructions. The transcribed RNAs were transfected into Vero cells using DMRIE-C, viruses were purified from the supernatant three or four days after transfection.

2.3. Ultra-high-performance liquid chromatography tandem mass spectrometry (UPLC-MS/MS)

UPLC-MS/MS was performed by Wuhan Metware Biotechnology Co., Ltd according to its suggested protocol. Briefly, after removing the cell debris, EV71 virions were collected by pelleting through 10% sucrose cushion via ultracentrifugation using a SW28Ti rotor (Beckman Coulter) at 115,900 rcf for 2 h at 4 °C. EV71 RNA was extracted using an RNeasy mini kit (Qiagen, Valencia, CA, USA), and digested into nucleosides by S1 nuclease (Takara, Shiga, Japan), alkaline phosphatase (Takara), and phosphodiesterase I (Sigma-Aldrich, St. Louis, MO, USA). The nucleosides were purified with phenol/chloroform and analyzed by the UPLC-ESI-MS/MS system (UPLC: ExionLC AD; MS: Applied Biosystems 6500 Triple Quadrupole). RNA modifications were analyzed using MetWare (http://www.metware.cn/) based on the AB Sciex QTRAP 6500 LC-MS/MS platform.

2.4. Dot-blot and western blot (WB)

Anti-m5C dot blot assays were performed as previously described (Arango et al., 2018). Briefly, RNA was extracted using TRIzol (Life technology), and 5 μg RNA was denatured for 5 min at 75 °C, chilled on ice for 1 min, loaded on Hybond-N^+ membranes, then subjected to the

ultraviolet crosslinking. Levels of m5C modifications were detected using anti-m5C Abs (Abcam, Cambridge, UK) and analyzed by the ChemiDoc MP imaging system (Bio-Rad Laboratories, Berkeley, CA, USA).

Cells were collected at the indicated times. And cell lysates were subjected to WB as described previously (Hao et al., 2017). The expression levels of target proteins were measured by indicated Abs.

2.5. RNA extraction, reverse transcription and qPCR (qRT-PCR)

After RNA extraction as described above, genomic DNA was digested with Turbo DNA kit (Life Technology). Reverse transcription was conducted with 1 μg RNA using a cDNA synthesis Kit (R111-02, Vazyme). Then, the qPCR was conducted using the Hieff qPCR SYBR Green Master Mix (11202ES03, Yeasen) on the CFX Connect Real-Time system (Bio-Rad). The thermocycling parameters were set as follows: 95 °C for 5 min, 40 cycles of 95 °C for 10 s and 55 °C for 20 s, then 72 °C for 20 s. Gene expression was quantified using the $2^{-\Delta\Delta Cq}$ method with Bio-Rad CFX Manager 3.0. For mRNA levels, relative gene expression of target genes was normalized with the gene expression of *GAPDH*. For Formaldehyde RIP-qPCR and MeRIP-qPCR, relative enrichment was normalized with inputs. The primers used in qRT-PCR assays can be found in Supplementary Table S1.

2.6. Formaldehyde-crosslinked RNA-immunoprecipitation (RIP) and m5C-Methylated RNA immunoprecipitation (MeRIP)

Formaldehyde-crosslinked RNA-immunoprecipitation (RIP) in RD cells was conducted as described previously (Hao et al., 2017). Briefly, cells were fixed by 1% formaldehyde (methanol-free) and quenched by 0.125 mol/L glycine. The fixed cells were lysed in RIP buffer, the supernatant was collected after centrifugated at 18,800 ×*g* for 10 min, which was subjected to overnight incubation with indicated Abs or control IgG by rotation at 4 °C. The pre-blocked protein-G agarose beads were added to each sample for 1 h incubation by rotation at 4 °C. Then, beads were washed three times with the washing buffer and the RIP buffer. After proteinase K digestion, indicated RNA samples were prepared after extraction by TRIzol.

M5C-methylated RNA immunoprecipitation (MeRIP) in RD cells was conducted briefly as previously described about m6A-MeRIP (Hao et al., 2019). Briefly, the extracted RNAs were incubated with anti-m5C Ab (Abcam) or control IgG Abs for 4 h by rotation at 4 °C. The anti-rabbit Abs conjugated magnetic beads (NEB, Ipswich, MA, USA; S1432S) were added to each sample for 2 h incubation by rotating for at 4 °C. Then, Beads were extensively washed six times with IP buffer and eluted by elution buffer for 1.5 h at 50 °C. The eluted RNAs were purified using phenol/chloroform and ethanol.

Above obtained RNA samples were subjected to RT-qPCR by indicated primers.

2.7. mRNA purification, nanopore sequencing, data processing and analysis

Total RNA was extracted using TRIzol reagent (Invitrogen). EV71 mRNAs along with host cell mRNAs were isolated by GenElute mRNA Miniprep Kit (Sigma-Aldrich) according to the manufacturer's instructions. The direct RNA sequencing was performed using Oxford Nanopore Technologies kit (the Oxford Nanopore DRS protocol, SQKRNA002) with the RCS control RNA, as previously described (Kim et al., 2020). The library for above poly A purified RNAs were prepared as the manufacturers' instructions (the Oxford Nanopore DRS protocol, SQKRNA002) suggested, and loaded on the FLO-MIN106D flow cell, followed by a 72 h sequencing run on a MinION device (Oxford Nanopore Technologies). The BENAGEN Company examined the Nanopore direct sequencing data using the EV71 XF strain's sequence as the viral reference genome. Multi-fast5 reads were base called using guppy (v3.1.5). Base called multi-fast5 reads were then converted to single read fast5s using command multi_to_single_fast5 by the Oxford Nanopore Technologies API, ont_fast5_api (v3.0.2). Single-fast5 data were then mapped to reference genome of EV71 using tombo (v1.5.1). The specific modifications were detected by tombo detect_modifications command and all-context alternate model identify 5-methylcytosine in any sequence context was used by running "–alternate-bases 5 mC". Then we use "text_output" command to get the methylation score and coverage rate at each position.

2.8. Immunofluorescence assay (IFA)

RD or Vero cells were seeded in confocal dishes 1 day before EV71 infection (MOI = 0.1) or transfection. After maintaining for indicated time, cells were washed three times with PBS and fixed in 4% paraformaldehyde for 10 min at 25 °C. After permeabilization with 0.1% Triton X-100 for 5 min, 3% bovine serum albumin was used for blocking for another 30 min. Then, cells were stained with indicated Abs for 2 h at 25 °C, after washing three times with PBS, cells were incubated with 1 μg/mL Alexa Fluor 488 (green) goat anti-rabbit IgG and/or Alexa Fluor 568 (red) goat anti-mouse IgG for another 1 h at 25 °C. The Hoechst was used to probe the cell nucleus. The distribution of target proteins was analyzed using a Perkin Elmer Ultraview Spinning Disk Confocal Microscope with a 60× objective lens. Indicated images from the same cell were merged using the same imaging software according to the manufacturers' instructions.

2.9. Co-immunoprecipitation (Co-IP) and ubiquitination assay

RD cells were collected at 48 h post-transfection, then washed with chilled PBS and lysed with chilled lysis buffer (50 mmol/L Tris-Cl, pH 7.5, 1 mmol/L EGTA, 1 mmol/L EDTA, 1% Triton X-100, 150 mmol/L NaCl, 2 mmol/L DTT) supplemented with protease Inhibitors. After incubating on ice for 30 min, the lysates were centrifuged at 18,800 ×*g* for 10 min, and the supernatant was collected. Supernatant (80 μL) was set as input, and the rest was proceeded to the following IP processes as previously described (Huang et al., 2022). The co-IP samples and input were denatured at 95 °C for 10 min and subjected to WB.

Ubiquitination assay was performed as previously described (Liu et al., 2016). HEK293T cells were collected at 48 h post-transfection, then washed with chilled PBS and lysed with above chilled lysis buffer supplemented with protease Inhibitors. The lysates were prepared as above mentioned. 80 μL of supernatant was set as input, and the rest was proceeded to the following IP experiments, same as above. The IP samples and input were denatured at 95 °C for 10 min, then subjected to WB.

2.10. Lentiviral based stable knockdown

The scramble shRNA or target genes specified shRNA were cloned into the lentiviral vector pLKO.1. After co-transfected with psPAX2 and pMD2.G into HEK293T cells, supernatants were collected and filtered through 0.45 μm filter-disks (Merck Millipore). RD cells were selected at a concentration of 2 μg/mL puromycin after transduced with above filtered lentiviruses for 48 h shRNAs used as follows: NSUN2 (shNSUN2-1: 5′-TGAGAAGATGAAGGTTATTAA-3′, shNSUN2-2: 5′-GAGCGATGCCTTAGGATATTA-3').

2.11. Ribosome loading assay

EV71 virus infected RD cells were firstly maintained with DMEM containing 100 μg/mL cycloheximide for 10 min. After washing twice with PBS, cells were lysed in ribosome lysis buffer (10 mmol/L Tris-HCl, pH 7.4, 5 mmol/L $MgCl_2$, 100 mmol/L KCl, 1% Triton X-100, Protease inhibitor, 2 mmol/L DTT, 100 mg/mL cycloheximide and RNase inhibitors). After centrifugated at 1300 ×*g* for 10 min, 10% of the supernatant were used as input, and the rest were loaded on top of 10%–50% gradient sucrose. After centrifugation at 164,000 ×*g* for 2 h at 4 °C, the

top lysis layer was removed, and RNA was extracted from ribosomal pellet layer using TRIzol. The viral RNA copy numbers were measured by RT-qPCR.

2.12. Mice, immunochemistry (IHC) and histopathological analysis

The 6 days old AG6 mice were randomly and equally divided into groups for EV71 infection. The handling of all mice was strictly in accordance with institutional guidelines and were approved by the Institutional Animal Care and Use Committee of WIV, CAS (Approval No. WIVA32202102).

Wuhan Servicebio Technology Co., Ltd. Performed IHC and histopathological analysis. Tissues taken from EV71 or DMEM challenged mice were promptly preserved in 4% PFA, embedded in paraffin, sectioned, and stained with hematoxylin and eosin for histological examination. For IHC, after blocking with PBS containing 3% BSA for 30 min at RT, the sections were incubated with anti-VP1 Abs (1:500) overnight at 4 °C. After washing three times with PBS, the sections were incubated with secondary Abs (horseradish peroxidase labeled) for 50 min at RT, and IHC was performed using diaminobenzidine chromogenic agent following the suggested protocols. Hematoxylin staining solution was used to counterstain the samples for 3 min. Images were obtained by Pannoramic DESK, P-MIDI, and analyzed by P250 (3D HISTECH).

2.13. Statistical analysis

Statistical analysis of qRT-PCR was performed using a two-tailed unpaired *t*-test in GraphPad Prism Software (La Jolla, CA, USA) (version 8). Data are presented as the means ± standard error of the mean (SEM) (n = 3). Results with P values of 0.05 or less were considered significant. The data presented in this study are representative of at least 3 independent experiments.

3. Results

3.1. EV71 RNAs harbor m5C modifications

Epitranscriptomic modifications, such as m6A and ac4C, on EV71 RNAs are essential for the replication of EV71 (Hao et al., 2019, 2022). To further explore the potential RNA modifications on EV71 RNAs, large-scale-cultured EV71 viruses were collected, and the purified viral RNAs were subsequently quantified via ultra-performance liquid chromatography-tandem mass spectrometry (UPLC-MS/MS). As presented in Fig. 1A, m5C residues among EV71 RNAs accounted for 0.0455% of the total cytidine. Subsequent dot blots with specific antibodies (Abs) against m5C were performed using T7 polymerase-transcribed full length EV71 RNAs *in vitro* or poly A purified viral RNAs extracted from EV71 virus-containing supernatants. The results indicated that purified EV71 RNAs contained m5C modifications, compared to *in vitro* transcribed RNAs (Fig. 1B). Additionally, methylated RNA immunoprecipitation (MeRIP) followed qRT-PCR analysis using RNAs extracted from EV71 infected RD cells showed that the EV71 RNAs were largely enriched by anti-m5C Abs, compared to the control IgG (Fig. 1C). To further map the exact m5C-modified ribonucleotides on EV71 RNAs, nanopore-based direct RNA sequencing was performed. Biometric analysis showed that the m5C-modified residues were mainly distributed at the 5′ end and coding sequence (CDS) region of the EV71 genome, and the common m5C sites rated with high score were identified in both EV71 infected Vero and RD cells (Fig. 1D and Supplementary Table S2). Thus, EV71 RNAs were found to possess m5C modifications during the viral replication.

The expression pattern of methyltransferases was reported to be affected by viral infection (Bohnsack et al., 2019). Levels of the methyltransferase NSUN2 proteins were increased in EV71-infected RD cells at 12 h post-infection (hpi) and 24 hpi, while other m5C related proteins DNMT2, ALYREF and YBX1 were not affected (Fig. 1E). Meanwhile, in EV71 infected RD cells, NSUN2 was found to translocate to the cytoplasm, and cytoplasmic NSUN2 co-localized with EV71 encoded VP1 proteins (Fig. 1F), compared to largely unaffected DNMT2 (Fig. 1G). Also, partial co-localization between ALYREF and VP1 was observed (Fig. 1H), and YBX1 shared moderate amount of co-localization with VP1 (Fig. 1I). Overall, EV71 RNAs harbored m5C modifications and EV71 infection altered the expression and localization of the m5C-associated host proteins.

3.2. NSUN2 along with m5C modifications promote EV71 replication

To reveal the roles of NSUN2 and m5C modifications during EV71 replication, levels of viral replication were measured in RD cells with depletion or over-expression of NSUN2. Exogenous NSUN2 increased levels of EV71 RNAs and the production of progeny viruses (Fig. 2A–C). In contrast, exogenous DNMT2 did not affect EV71 replication (Supplementary Fig. S1A and S1B). Levels of m5C-modified EV71 RNAs were increased in RD cells with overexpressed NSUN2 according to RNA IP using anti-m5C Abs (Fig. 2D), and NSUN2 was found to associate with EV71 RNAs via formaldehyde cross-linked RNA IP with anti-NSUN2 Abs (Fig. 2E). Furthermore, NSUN2 depletion decreased EV71 RNA levels and progeny virus production (Fig. 2F–H). Levels of m5C modifications on EV71 RNAs were also decreased in NSUN2-knockdown (shNSUN2-1/2) RD cells with the indicated shRNAs (Fig. 2I and J). Both ALYREF and YBX1 as reader proteins recognize m5C modified residues, which is involved in the nuclear export and stability of m5C-containing transcripts (Yang et al., 2017; Feng et al., 2021). However, overexpression of these two reader proteins did not affect EV71 replication (Supplementary Fig. S1C–S1F).

The dominant negative (DN) NSUN2 (NSUN2-C321A) has been reported to be loss of the catalytic activities (Hussain et al., 2013). The introduction of DN NSUN2 results in competition with endogenous NSUN2 to bind the indicated targets without catalyzing subsequent m5C modifications. As presented in Fig. 2K and L, over-expressed NSUN2-C321A led to decreased m5C-modified EV71 RNA levels in RD cells. Thus, NSUN2 catalyzed the m5C modification of EV71 RNAs and promoted the viral replication.

Functional RNA modifications have been shown to facilitate viral replication (Hao et al., 2019; Hao et al., 2022). To determine whether all four m5C modified sites contribute to EV71 replication, mutant EV71 viruses bearing the substitutions of indicated cytosine (nt 584, 1460, 2637 and 7009) were generated. To maintain the intact secondary structure of the IRES motif, the guanine at nt 621 was substituted with cytosine in Mut-584 plasmid. The mutation nt 1460 did not lead to amino acids change, while the substitutions at nt 2637 and 7009 did (Fig. 2M and Supplementary Fig. S2A). All four mutant EV71 viruses exhibited reduced replication efficiency compared to that of the WT viruses (Fig. 2N and O, Supplementary Fig. S2B). In addition, the production of progeny mutant EV71 viruses (Mut-584 and Mut-1460) was reduced in RD cells with scramble shRNA (shNC) (Fig. 2P, left 3 bars), whereas such affects were diminished by NSUN2 depletion (Fig. 2P, right 6 bars). Taken together, above results revealed that NSUN2 and m5C modifications were essential for EV71 replication.

3.3. m5C modifications enhance translation efficiency and stability of EV71 RNA

m5C modifications catalyzed by NSUN2 affect the trafficking, translational efficiency, and stability of viral RNAs (Schumann et al., 2020). Consistently, mutant EV71 viruses (Mut-584 and Mut-1460) exhibited lower expression of VP1 proteins compared to that of WT EV71 viruses (Fig. 3A). Exogenous NSUN2 promoted the expression of EV71-encoded VP1 protein (Fig. 3B). To determine whether the m5C modifications would affect translation efficiency, the amount of ribosome-loaded EV71 RNAs was measured in RD cells in the presence or absence of NSUN2. The results revealed that the ribosome-loading capacities of EV71 RNAs were enhanced by NSUN2 over-expression (Fig. 3C). In contrast, knockdown

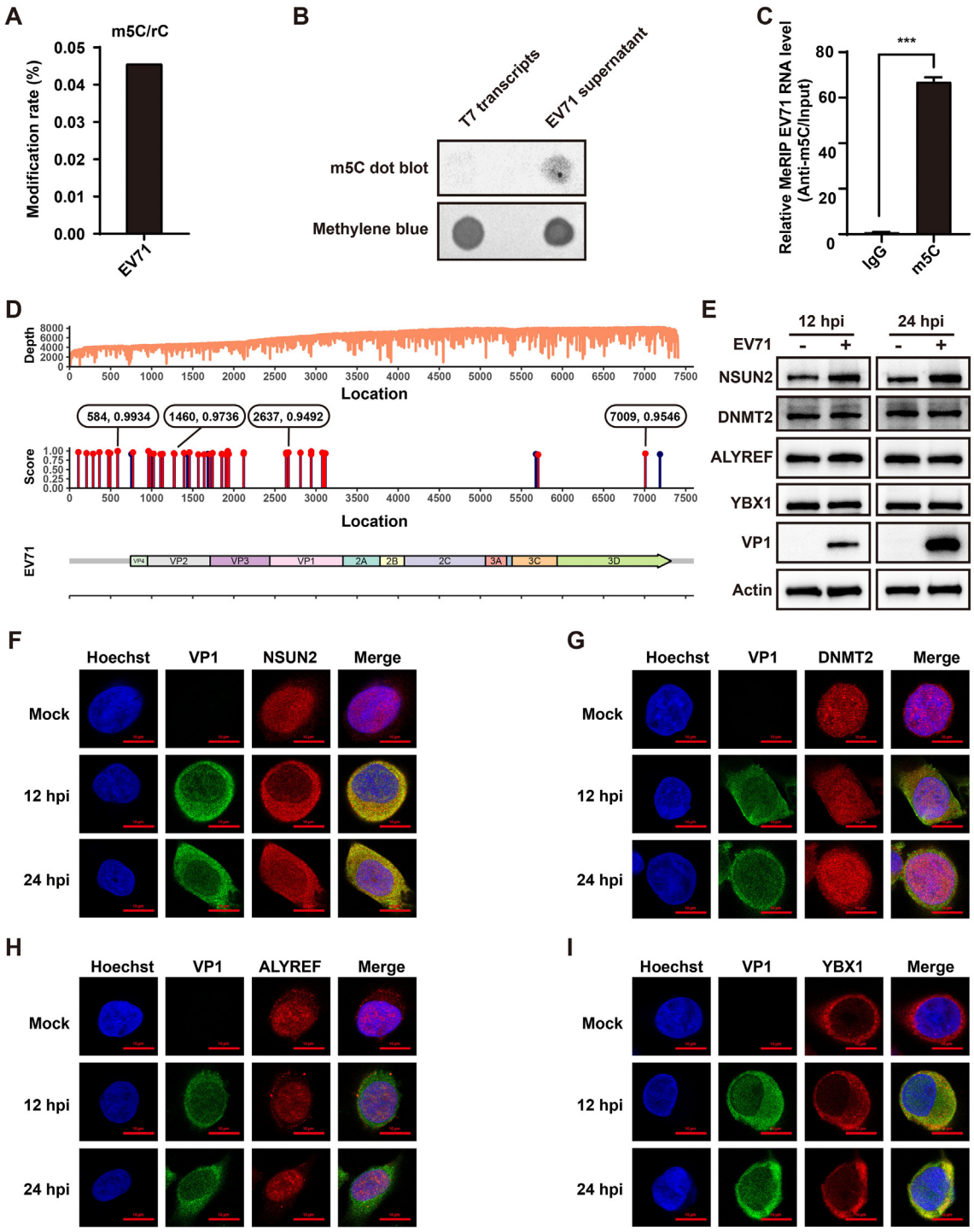

Fig. 1. Enterovirus 71 (EV71) RNA harbors 5-methylcytosine (m5C) modifications and m5C-related proteins are altered by EV71 infection. **A–D** EV71 RNAs were found to harbor m5C modifications. **A** The ratio of m5C modifications among all cytidines in the EV71 RNA extracted from viral particles was analyzed via ultra-performance liquid chromatography-tandem mass spectrometry (UPLC-MS/MS) and presented as a bar graph. **B** m5C dot blot was conducted between *in vitro* transcribed EV71 RNA and poly A purified viral supernatant RNA using anti-m5C antibodies (Abs) and methylene blue staining. **C** Methylated RNA immunoprecipitation (MeRIP) was conducted using purified mRNA from EV71-infected Vero cells with control IgG or anti-m5C Abs, and levels of EV71 RNA were measured by RT-qPCR. An unpaired Student's *t*-test was performed, and data are presented as the means ± SEMs (n = 3). ***$P \leq 0.001$. **D** Direct RNA sequencing was conducted using the poly A-purified RNAs from EV71-infected Vero cells and RD cells. The top bar graphs present the 'depth' and indicated 'score' of the sequencing output, and the bottom diagram presents EV71 genome. Red lines in middle bar graph present common m5C modified sites in both cells, while blue lines present different ones. The sites presented in the graph all score more than 0.9. **E** EV71 infection altered the expression of m5C-related proteins. Levels of NSUN2, DNMT2, ALYREF, YBX1, VP1 and Actin were measured using indicated Abs at 12 h and 24 h in RD cells infected with EV71 or not. **F–I** EV71 infection affected the distribution of m5C-related proteins. The localization of NSUN2 (**F**), DNMT2 (**G**), ALYREF (**H**), and YBX1 (**I**) proteins probed using indicated Abs are presented as red, VP1 protein probed using anti-VP1 Abs is presented as green, and nucleus stained using Hoechst is presented as blue in RD cells at 0, 12 and 24 h after EV71 infection. The exact distribution of indicated proteins is presented as the 'merge' image. Scale bar, 10 μm.

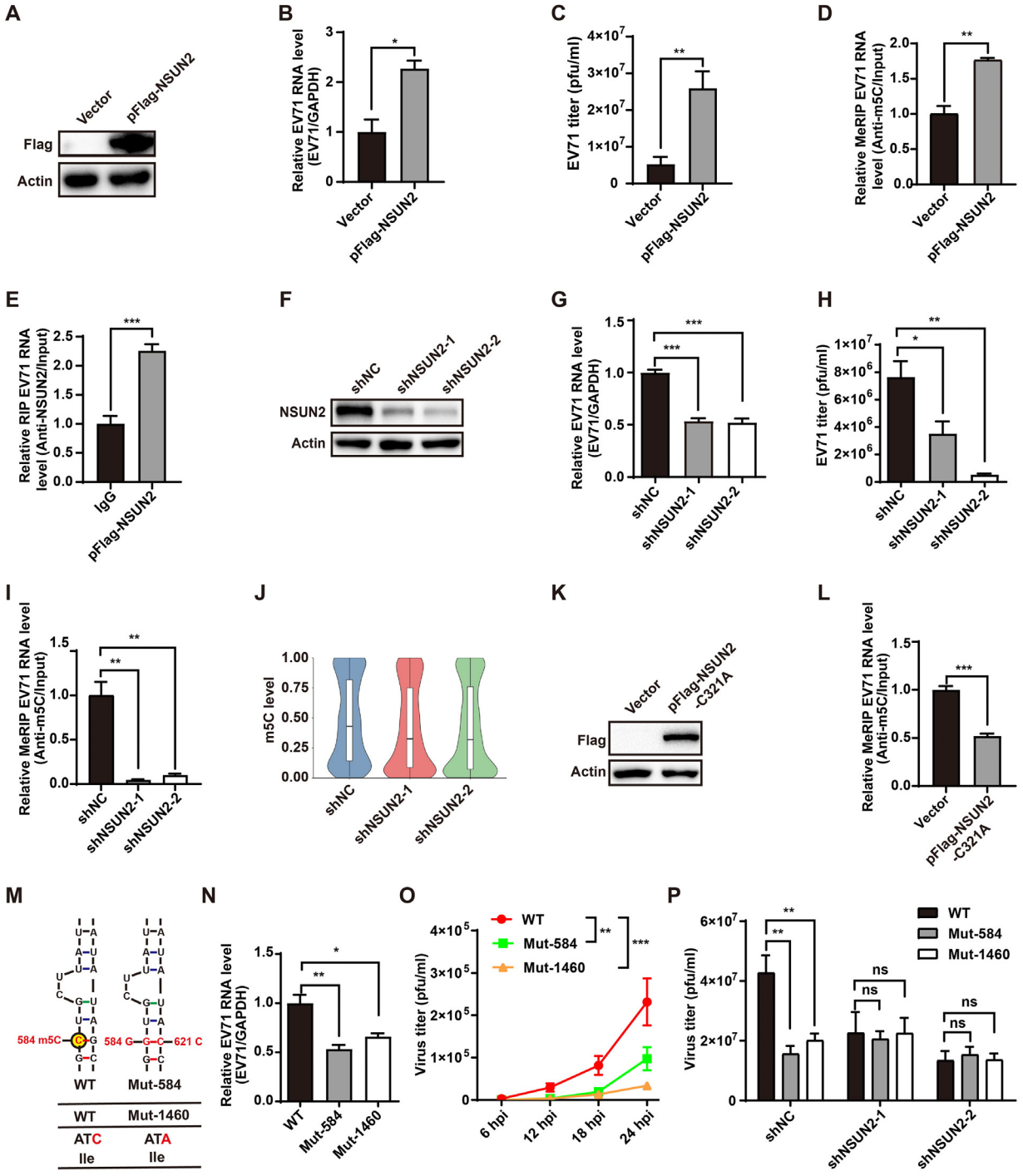

Fig. 2. NSUN2 and m5C modifications promote EV71 replication. **A–E** Exogenous NSUN2 increased the replication and levels of m5C modifications on EV71 RNAs. **A** Levels of exogenous NSUN2 and Actin were measured in RD cells. Levels of EV71 RNAs were quantified (**B**) and numbers of progeny EV71 particles were titrated (**C**) in EV71 infected RD cells with/without exogenous NSUN2 and presented as bar graphs. Levels of m5C-modified (**D**) or NSUN2-specifically bound (**E**) EV71 RNAs were quantified in RD cells from (**B** and **C**) and presented as bar graphs. **F–J** Depletion of NSUN2 decreased the replication and levels of m5C modifications on EV71. **F** Levels of NSUN2 and Actin were examined in RD cells with scramble shRNA (shNC) or two different NSUN2-specific shRNAs (sh-NSUN2-1 and sh-NSUN2-2). Levels of EV71 RNAs were quantified (**G**) and numbers of progeny EV71 particles were titrated (**H**) in RD cells from (**F**) and presented as bar graphs. Levels (**I**) and the exact ratios (**J**) of m5C-modified EV71 RNAs were measured in RD cells from (**F**) and presented as bar graphs. **K, L** The dominant negative NSUN2/C321A decreased levels of m5C-modified EV71 RNAs. **K** Levels of NSUN2/C321A and Actin were measured in RD cells. **L** Levels of m5C-modified EV71 RNAs were quantified in EV71 infected RD cells with/without exogenous NSUN2/C321A and presented as a bar graph. **M–P** Mutant EV71 strains lacking the indicated m5C-modified residues exhibited markedly reduced viral replication. **M** Mut-584 (top diagrams) and Mut-1460 EV71 (bottom panels) strains were presented. EV71 RNA levels at 12 h (**N**), numbers of progeny viruses (**O**) in RD cells infected with WT or two mutant EV71 strains were measured at multiple time points (0, 6, 12, 18 and 24 h) and presented as bar graphs or line chart. **P** Numbers of progeny EV71 particles in WT or two mutant EV71 viruses-infected RD cells with shNC, shNSUN2-1, or shNSUN2-2 were measured at 24 h and presented as a bar graph. Unpaired Student's *t*-tests were performed for all bar graphs, and data are presented as the means ± SEMs (n = 3). $^{*}P \leq 0.05$, $^{**}P \leq 0.01$. ns: not significant. For (O), data are means ± SEMs (n = 3). $^{**}P \leq 0.01$, $^{***}P \leq 0.001$. Two-way ANOVA.

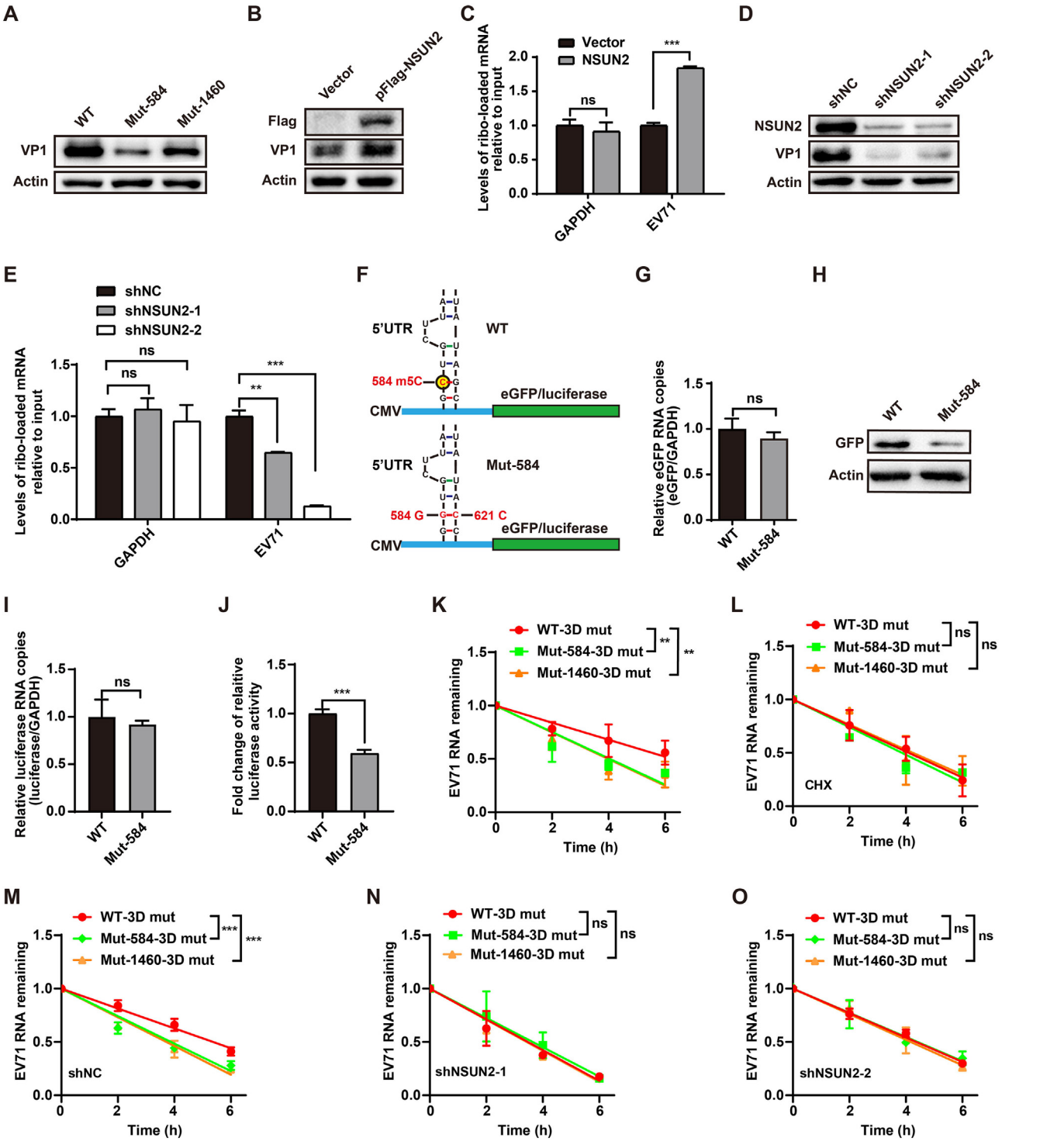

(caption on next page)

Fig. 3. m5C modifications in the IRES motif enhances translation efficiency and facilitate EV71 RNA stability.
A Mutant EV71 strains exhibited lower viral protein expression. Levels of VP1 and Actin were measured at 12 h in RD cells infected with WT or two mutant EV71 (Mut-584 and Mut-1460) strains using the indicated antibodies (Abs). **B, C** Exogenous NSUN2 promoted viral protein expression by enhancing ribosome loading capacity. **B** Levels of NSUN2, VP1 and Actin were measured in EV71-infected RD cells with over-expressed NSUN2 or not using the indicated Abs. **C** Levels of ribosome-bound GAPDH or EV71 RNAs were relatively quantified in RD cells from (**B**) and presented as a bar graph. **D, E** The depletion of NSUN2 decreased viral protein expression by inhibiting ribosome-loading capacity. **D** Levels of NSUN2, VP1 and Actin were measured in EV71-infected RD cells with shNC, shNSUN2-1 or shNSUN2-2 using the indicated antibodies. **E** Levels of ribosome-bound GAPDH or EV71 RNAs were relatively quantified in RD cells from (**D**) and presented as a bar graph. **F–J** m5C modifications in the IRES motif of the 5′ UTR promoted ribosome loading. **F** The diagram of indicated reporter systems with the WT or mutant (584 and 621) 5′ UTR between the CMV promoter and the coding sequences (CDS) of reporter genes. **G** Levels of eGFP RNA were quantified in RD cells transfected with indicated chimeric eGFP plasmids and presented as a bar graph. **H** Levels of eGFP and Actin were measured in RD cells from (**G**) using the indicated Abs. **I** Levels of firefly luciferase (fLuc) RNA were quantified in RD cells co-transfected with indicated chimeric luciferase plasmids and a Renilla luciferase (rLuc) plasmid, and presented as a bar graph. **J** Levels of fLuc activities were quantified relative to rLuc activities in RD cells from (**I**) and presented as a bar graph. Unpaired Student's *t*-tests were performed for all bar graphs, and data are presented as the means ± SEMs (n = 3). $^{***}P \leq 0.001$. ns: not significant. **K–O** Mutant EV71 strains lacking m5C-modified resides exhibited lower viral RNA stability. In vitro T7-transcribed WT-3D mut, Mut-584-3D mut or Mut-1460-3D mut RNAs were transfected into RD cells in the presence of CHX (**L**) or not (**K**), or with depletion of NSUN2 (**N** and **O**) or not (**M**). Level of EV71 RNAs at the indicated time points post-transfection (3 h post-transfection was set as '0 h') were measured, and the indicated decay graphs were generated by applying the linear regression analysis. Data are means ± SEMs (n = 3). $^{**}P \leq 0.01$, $^{***}P \leq 0.001$, ns: not significant, two-way ANOVA.

of NSUN2 led to the decrease of both VP1 protein levels (Fig. 3D) and the ribosome-loading capacities on EV71 RNAs (Fig. 3E). These data indicated that NSUN2 promoted the translational efficiency of EV71 transcripts by catalyzing m5C modifications on its RNAs.

The m5C modification at nt 584 Is located in stem-loop VI (nt 566–636) within the IRES motif of the 5′ UTR, which is essential for the translation of viral proteins (Lin et al., 2008; Sweeney et al., 2014). To determine whether m5C at nt 584 affected the translation efficiency of EV71 RNAs, the reporter plasmids were constructed by inserting the above WT or m5C mutant 5′-UTR between the promoter and reporter protein eGFP or a luciferase expression cassette (Fig. 3F). Notably, the expression of the reporter genes (GFP and luciferase) was reduced in m5C mutants compared to that of wild types (Fig. 3H and J), while the RNA levels were not affected (Fig. 3G and I). Thus, the m5C modification of nt 584 enhanced the translation efficiency of EV71 RNAs.

RNA modifications were reported to affect RNA translation and stability (Chen et al., 2021; Gao and Fang, 2021). To determine whether EV71 m5C modifications affected viral RNA stability, replication-deficient infectious clones with WT and m5C mutations were constructed, in which 3D polymerase was code-shift mutated. *In vitro* transcribed full-length EV71 RNAs was transfected into RD cells for stability experiments. The RNA degradation was stronger in the m5C-mutant EV71 cells than that of WT (Fig. 3K). CHX blocks global translation in cells. Similarly, the stability of WT and m5C-mutant strains did not differ when cells were treated with CHX (Fig. 3L). However, no differences of the RNA degradation rates were observed between the WT and m5C mutants in NSUN2 knockdown cells (Fig. 3M–O). These results suggested that the m5C modification of EV71 RNAs enhanced translational efficiency, and further promoted RNA stability.

3.4. NSUN2 targets EV71 VP1 protein for binding and promotes its stability

To investigate the mechanism how NSUN2 facilitated the EV71 replication, NSUN2-associated proteins in EV71 virus-infected RD cells were pulled down with specific Abs and analyzed via mass spectrometry. The structural protein VP1 was ranked among the top candidates (Supplementary Fig. S3A) and was detected within the NSUN2-precipitated mixture (Fig. 4A). The interactions between NSUN2 and VP1 was confirmed by co-IP experiments in NSUN2- and VP1-over-expressing RD cells with or without RNase A treatment (Fig. 4B and Supplementary Fig. S3B–S3D). Meanwhile, NSUN2 was found to translocate to the cytoplasm in the presence of exogenous VP1 expression and co-localize with VP1 in RD cells (Fig. 4C). To reveal the potential effects on VP1 proteins mediated by NSUN2, VP1 was co-expressed with increasing amounts of NSUN2 in RD cells. The expression of VP1 protein was increased in a dose-dependent manner (Fig. 4D). In contrast, levels of NSUN2 were unaffected by the increasing expression of VP1 (Supplementary Fig. S3E).

To further characterize the mechanisms underlying the increased expression of VP1 induced by NSUN2, a pulse-chase experiment was conducted by using cycloheximide (CHX). VP1 exhibited a very short half-life (~2 h) in RD cells and the abundance was quickly diminished after treatment with CHX (Fig. 4E). The similar phenomenon was observed in virus-infected RD cells (Fig. 4F). Additionally, the degradation of VP1 was found to be mediated by ubiquitination, which was enhanced after treating with proteasomal inhibitor MG132 (Fig. 4G). To explore the exact mechanisms how NSUN2 promoted the stability of VP1, the N-terminus and C-terminus truncated VP1 were constructed to identify the exact ubiquitinated region. As presented in Fig. 3H, the ubiquitinated residues mainly located within the N-terminus of VP1, compared to the full length (FL) and N-terminus truncated VP1. Furthermore, co-IP experiments conducted between NSUN2 and FL or the two truncated VP1 proteins revealed that the N-terminus of VP1 was targeted by NSUN2 for binding (Fig. 4I and Supplementary Fig. S3F). And the ubiquitination levels of VP1 were reduced in the presence of exogenous NSUN2 (Fig. 4J). K48-linked polyubiquitination is the most common consequence of proteasome-mediated degradation (Lopata et al., 2020). In addition, the effects of NSUN2 affecting the K48-linked ubiquitination of VP1 were measured, which showed that NSUN2 inhibited K48-linked ubiquitination levels of VP1 (Supplementary Fig. S3G). These results indicated that NSUN2 targeted the N-terminus of VP1 for binding and promoted its stability by inhibiting K48-linked polyubiquitination.

3.5. m5C modifications influence the pathogenicity of EV71 in mice

RNA modifications, such as m6A in influenza and ac4C on EV71 RNAs, have been linked to viral pathogenicity (Courtney et al., 2017; Hao et al., 2022). To investigate whether m5C modifications on EV71 RNAs affected viral pathogenicity, AG6 interferon receptor-deficient mice were infected with WT, Mut-584, or Mut-1460 EV71 viruses. The survival time, viral loads in different organs, and pathological changes in multiple organs were measured separately. Mice infected with mutant EV71 viruses (Mut-584 or Mut-1460) had longer survival times (Fig. 5A and Supplementary Fig. S4A) than those infected with the WT virus. Additionally, the viral loads, quantified by qRT-PCR assays using different organs obtained from mice infected with mutant EV71 viruses for 48 hpi or 72 hpi, showed a consistent decrease (Fig. 5B–F and Supplementary Fig. S4B–S4F), compared to that of WT EV71 infected mice. It is well documented that pathogenicity is mostly correlated with viral replication. Hematoxylin and eosin staining was performed to determine the histological abnormalities in the intestines, brains, and hindlimbs of

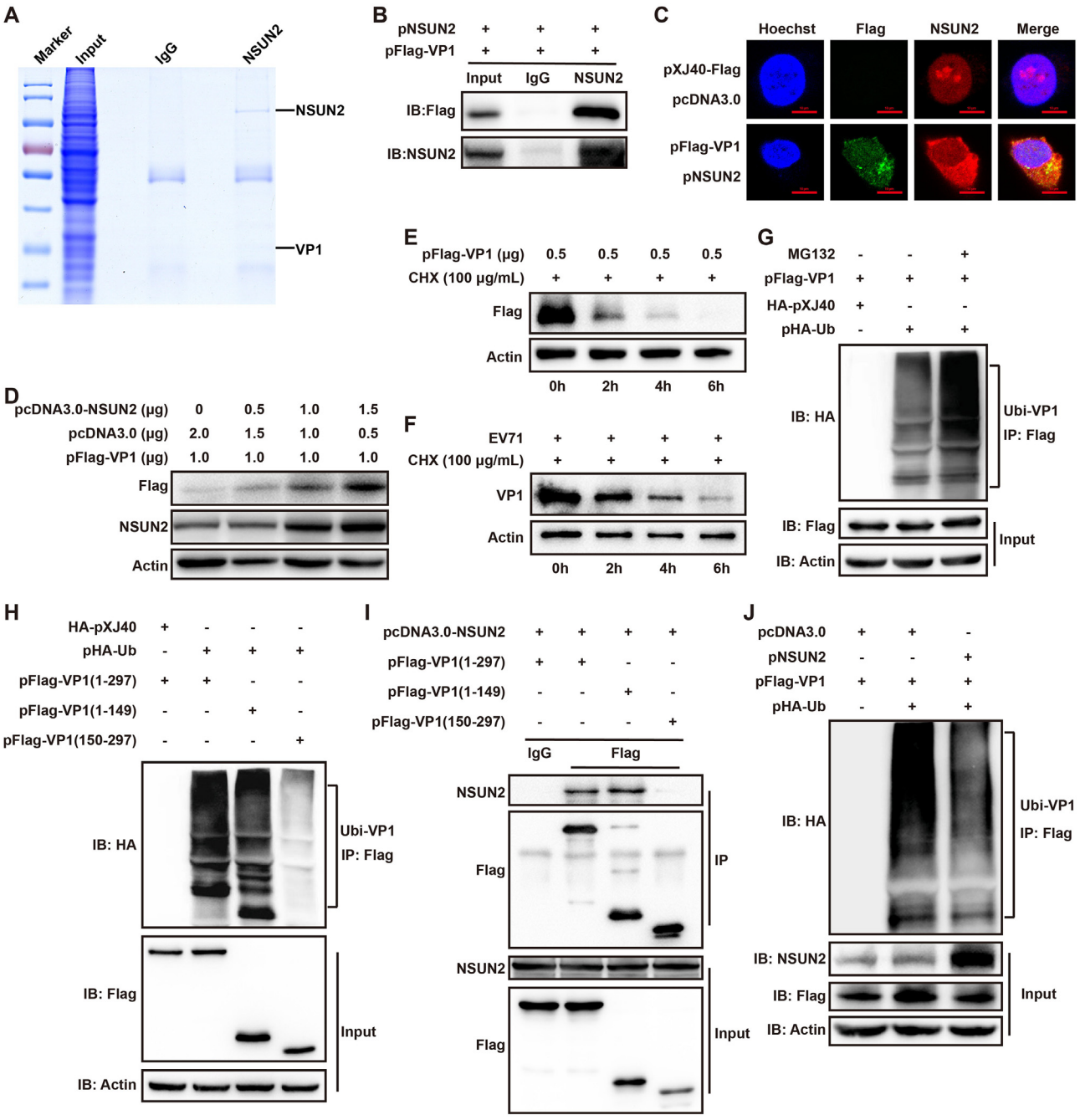

Fig. 4. NSUN2 interacts with EV71 VP1 protein and promotes its stability by inhibiting polyubiquitination. **A–C** NSUN2 targets VP1 for binding. **A** IP samples obtained from EV71-infected RD cells with over-expressed NSUN2 using anti-NSUN2 antibodies (Abs) or control IgG, as well as the indicated input, were subjected to SDS-PAGE and then Coomassie blue staining. **B** Co-IP using anti-NSUN2 Abs and input samples obtained from RD cells with over-expressed NSUN2 and VP1 were examined using the indicated Abs. **C** The localization of exogenous NSUN2 and VP1 proteins was probed using the indicated Abs and presented as red and green colors, respectively, and the nuclei were stained with Hoechst and presented as blue. The exact distribution of NSUN2 and VP1 is presented as the 'merge' image. Scale bar, 10 μm. **D** NSUN2 promoted the expression of VP1 in a dose-dependent manner. Levels of NSUN2, VP1 and Actin were measured in RD cells transfected with constant amount of VP1 plasmid and increasing amount of NSUN2 plasmid. Empty vectors were supplemented for equal amounts of transfected plasmids. **E–G** VP1 is degraded in the ubiquitination mediated proteasomal pathway. Levels of over-expressed (**E**) or EV71-encoded (**F**) VP1 proteins and Actin were measured in RD cells after treating with cycloheximide (CHX) for the indicated time (0, 2, 4, 6 h). **G** IP samples were obtained from HEK293T cells with over-expressed VP1 and ubiquitin in the presence of MG132 or not using anti-Flag Abs. Levels of VP1 ubiquitination were measured using anti-HA Abs. The input samples were measured using the indicated Abs. **H–J** NSUN2 targets N-terminus of VP1 for binding and inhibits its ubiquitination. **H** IP samples were obtained from HEK293T cells with over-expressed VP1 or two truncated VP1 [VP1(1–149) and VP1(150–297)] and ubiquitin using anti-Flag Abs. Levels of VP1 ubiquitination were measured using anti-HA Abs, and the input samples were measured using the indicated Abs. **I** Co-IP samples were obtained from HEK293T cells with over-expressed NSUN2 and VP1 or the two truncated mutants. Proteins were detected using the indicated Abs. **J** IP samples were obtained from HEK293T cells with over-expressed VP1 and ubiquitin in the presence of exogenous NSUN2 or not using anti-Flag Abs, levels of VP1 ubiquitination were measured using anti-HA Abs. The input samples were measured using the indicated Abs (bottom 3 panels).

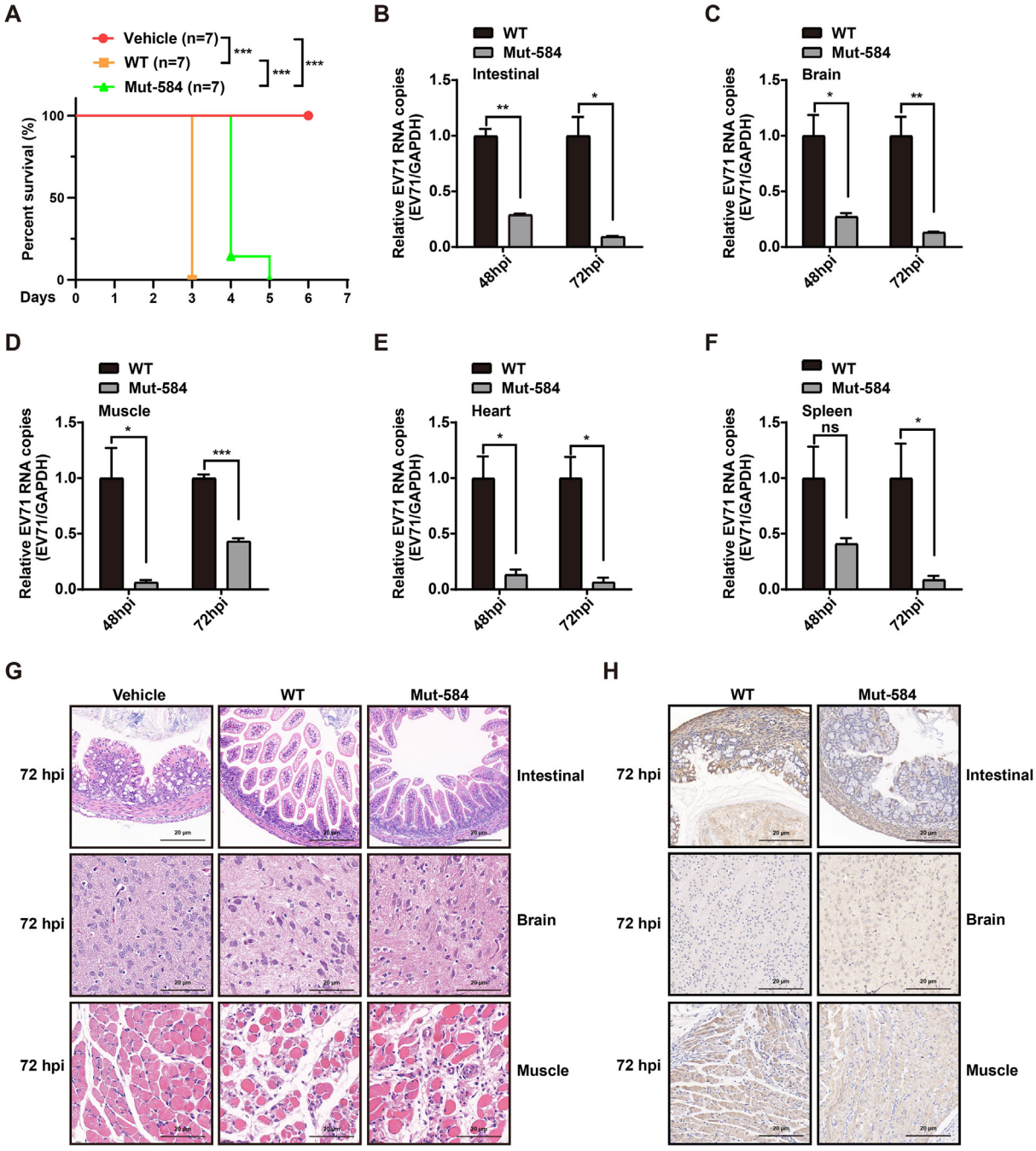

Fig. 5. A mutant enterovirus 71 (EV71) strain (Mut-584) lacking 5-methylcytosine (m5C)-modified residues exhibits significantly attenuated pathogenicity in mice. **A** Mice were separately challenged with the same numbers (10^5 PFU) of WT (yellow) or m5C-mutant (Mut-584) (green) EV71 strains, and DMEM was set as control (vehicle) (red). Each group consisted of seven mice, and the indicated survival time was measured and presented as a line chart. A log-rank (Mantel-Cox) test was performed (***$P \leq 0.001$). **B–F** After euthanizing AG6 mice challenged with WT or Mut-584 EV71 strains for 48 h or 72 h, levels of viral RNAs in intestinal (**B**), brain (**C**), muscle (**D**), heart (**E**), spleen (**F**), and samples were quantified and presented as bar graphs. Unpaired Student's *t*-tests were performed for all bar graphs, and data are presented as the means ± SEMs (n = 3). *$P \leq 0.05$, **$P \leq 0.01$. ns: not significant. **G, H** After challenging mice with DMEM (vehicle) or WT or Mut-584 EV71 viruses for 72 h, hematoxylin and eosin staining (**G**) or immunohistochemistry to detect (**H**) EV71 particles using anti-VP1 Abs was performed on the intestine (top panel), brain (middle panel), and limb muscle (bottom panel) samples. The scale bar is 20 μm.

mice. As presented in Fig. 5G and Supplementary Fig. S4G, compared to those phenotypes in animals infected with WT EV71, intestinal lesions produced fewer vacuoles, the degree of brain neuron loss was reduced, and the rhabdomyocytes were less dissolved in mice infected with mutant EV71 viruses at 72 hpi. Furthermore, lower VP1 expression was detected in the organs of mutant EV71 virus-infected mice (Fig. 5H and Supplementary Fig. S4H). The above results revealed that m5C modifications were pivotal for EV71-induced pathogenicity in mice.

4. Discussion

NSUN2 and its catalyzed m5C modifications have been shown to regulate the replication of different viruses (Motorin and Helm, 2011; Imam et al., 2020). However, other potential roles of NSUN2 along with m5C modifications are poorly elucidated. In this study, NSUN2 was not just characterized as a methyltransferase that catalyzed m5C modifications on EV71 RNAs, but also was revealed to affect multiple steps during

EV71 replication. NSUN2 was found to interact with VP1 and promote the protein stability by inhibiting its ubiquitination. Thus, NSUN2 and its catalyzed functional m5C-modified residues on EV71 RNAs are vital for viral replication in cells and pathogenicity in mice.

Here, the functional NSUN2 catalyzed m5C-modified residues of EV71 RNAs were confirmed by mutating these identified sites in infectious clones. As cytidine 584 is located in the IRES motif of the 5′ UTR, symmetric substitutions of cytidine 584 and its paired guanosine 621 abolished m5C modifications on cytidine 584 but maintained the intact stem structure of the IRES motif of the 5′ UTR. The other three m5C-modified residues were found to be located within the CDS region of the EV71 genome. Whereas only the substitution for cytidine 1460 was synonymous, the other three cytidine substitutions led to changes in the amino acids. Due to the potential effects caused by changes in amino acids, only cytidines 584 and 1460 were investigated to decipher the exact roles of m5C modifications in EV71 replication. Indeed, the substitutions of these two cytidines resulted in a decrease in viral replication, which was caused by the inhibition of translation efficiency and RNA stability. Thus, similar as previous studies, NSUN2 and its catalyzed m5C modifications were also revealed to positively regulate EV71 replication.

Numerous studies revealed that "writer" proteins not only catalyze the modifications of viral RNAs but also participate in the regulation of viral replication by targeting viral proteins. The methyltransferase METTL3, which catalyzes m6A modifications of EV71 RNAs, was demonstrated to target the EV71 RdRp 3D protein to affect its ubiquitination and further promote EV71 replication (Hao et al., 2019). The RdRp of SARS-CoV-2 was reported to inhibit the sumoylation and ubiquitination levels of METTL3, which resulted in the enhanced m6A modification of viral RNA (Zhang et al., 2021). NSUN2 was found to interact with the viral structural protein VP1 in an RNA-independent manner. The degradation of exogenous or EV71-encoded VP1 protein was revealed in our study, and expression of NSUN2 was able to inhibit such degradation. To be noticed, EV71 encoded VP1 proteins did possess longer half-life in the pulse chase assays, compared to the overexpressed VP1 proteins. Such differences were caused by the capsid complex formed by VP1 and other structural proteins, which potentially blocked the degradation. In addition, NSUN2 stabilized the VP1 protein by inhibiting its K48-linked ubiquitination. Along with other studies showing that the "writer" proteins target viral proteins to regulate viral replication, it will not be surprising if more RNA modification-related proteins are characterized with novel functions beyond the enzymatic activities during the viral replication in future studies.

Previous studies have revealed that m6A modification of the influenza virus and ac4C modification of the EV71 virus have been reported to affect the viral pathogenicity in mice (Courtney et al., 2017; Hao et al., 2022). Mice infected with the mutant EV71 strain, with a substitution at the ac4C modification site, have prolonged survival times, and this virus exhibits lower pathogenicity (Hao et al., 2022). We found that mice infected with mutant EV71 viruses lacking m5C-modified residues survived longer. Meanwhile, these mutant EV71 virus-infected mice exhibited decreased EV71 replication and reduced pathogenic effects in

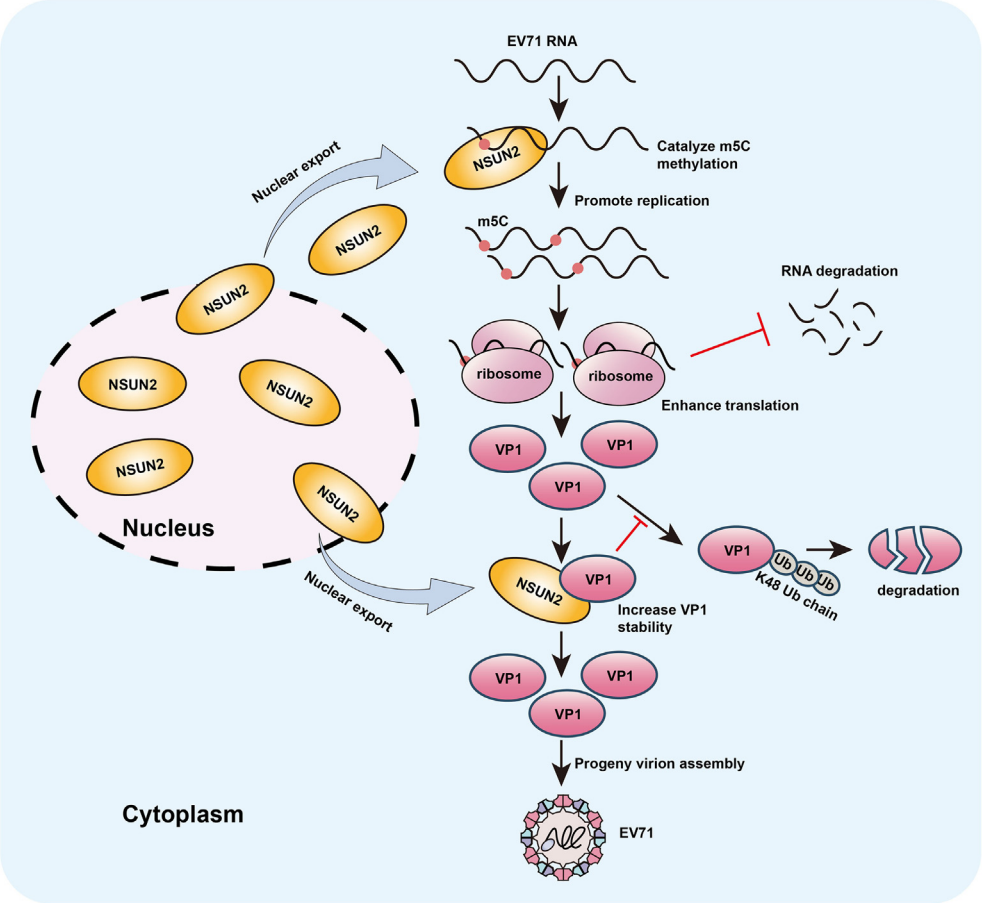

Fig. 6. The schema diagram illustrates the molecular mechanisms how NSUN2 and m5C modifications regulate EV71 replication. After EV71 infection, NSUN2 was translocated to cytoplasm, and catalyzed m5C modifications of viral RNA. The m5C modified EV71 mRNA showed enhanced translation of viral encoded proteins by increasing its ribosome-loading capacity, which in turn promoted the stability of viral RNA. VP1 protein was found to be K48-linked poly-ubiquitinated and degraded, while NSUN2 was capable to target VP1 for binding and reverse its degradation. Thus, NSUN2 and its catalyzed m5C modification on EV71 RNAs promote the viral replication.

multiple organs *in vivo*. These results reveal that m5C modifications affect viral pathogenicity by regulating EV71 replication, which will provide a novel therapeutic target in the clinic.

5. Conclusions

Taken together, functional m5C sites on EV71 RNAs were identified within the IRES motif and CDS region, which promoted the translational efficiency and stability of viral RNAs. In addition, a new role of NSUN2 was characterized that it targeted viral protein VP1 for binding, leading to enhance the stability of VP1 by inhibiting its K48-linked poly-ubiquitination (Fig. 6). Furthermore, the m5C modifications on EV71 RNAs were demonstrated to play pivotal roles in the EV71 pathogenicity in mice. Besides, the importance of m5C modifications in other viruses needs to be studied, which will help to elucidate how epitranscriptomic modifications participate in the regulation of viral replication and host-cell metabolism. Thus, our study provided new insights for epitranscriptomic researches during viral replication, and revealed potential therapeutic values to prevent and treat EV71 infection in clinic, by targeting the viral RNA modifications.

Data availability

The complete CDS sequence of EV71 (strain XF) used in this work has been deposited with National Center for Biotechnology Information under accession number JQ804832. Original data and materials will be available upon requests.

Ethics statement

Every procedure and protocol involving animals were permitted by the Wuhan Institute of Virology, Chinese Academy of Science (Approval Number: WIVA32202102, date: April 3rd, 2021). The study was based on the Guide to moral Control and Supervision in Animal Conservation and use.

Author contributions

Lishi Liu: Data curation, Formal analysis, Investigation, Methodology, Writing–original draft. Zhen Chen: Data curation, Investigation. Kui Zhang: Data curation. Haojie Hao: Methodology. Li Ma: Formal analysis. Haizhou Liu: Formal analysis. Baocheng Yu: Data curation. Shuang Ding: Resources. Xueyan Zhang: Data curation. Miao Zhu: Data curation. Xiang Guo: Data curation. Yi Liu: Resources. Haibin Liu: Supervision. Fang Huang: Funding acquisition, Supervision, Writing-review & editing. Ke Peng: Resources, Supervision, Writing-review & editing. Wuxiang Guan: Conceptualization, Funding acquisition, Project administration, Supervision, Writing-review & editing.

Conflict of interest

The authors declare that they have no conflict of interest.

Acknowledgements

This study was supported by the National Natural Science Foundation of China (31970168), the Key R&D Program of Hubei Province (2021BCD004), the Hubei Central Leading Local Science and Technology Special Project (2022BGE245), the Hubei Science and Technology Major Project [2021ACB004], and the Wuhan Knowledge Innovation Special Project (2023020201020303).

We thank Lei Zhang, Pei Zhang and Ding Gao of the 'Core Facility and Technical Support' in the Wuhan Institute of Virology (WIV), Chinese Academy of Sciences (CAS) for the help in maintaining ultracentrifugation and confocal microscopy. We also thank Xuefang An, Yuzhou Xiao, Li Li, Fan Zhang and He Zhao of the 'Center for Animal Experiment' of WIV, CAS for the help in handling the mice experiments.

Appendix A. Supplementary data

Supplementary data to this article can be found online at https://doi.org/10.1016/j.virs.2024.05.002.

References

Arango, D., Sturgill, D., Alhusaini, N., Dillman, A.A., Sweet, T.J., Hanson, G., Hosogane, M., Sinclair, W.R., Nanan, K.K., Mandler, M.D., Fox, S.D., Zengeya, T.T., Andresson, T., Meier, J.L., Coller, J., Oberdoerffer, S., 2018. Acetylation of cytidine in mRNA promotes translation efficiency. Cell 175, 1872–1886 e1824.

Bohnsack, K.E., Hobartner, C., Bohnsack, M.T., 2019. Eukaryotic 5-methylcytosine (m(5)C) RNA methyltransferases: mechanisms, cellular functions, and links to disease. Genes 10, 102.

Cardosa, M.J., Perera, D., Brown, B.A., Cheon, D., Chan, H.M., Chan, K.P., Cho, H., McMinn, P., 2003. Molecular epidemiology of human enterovirus 71 strains and recent outbreaks in the Asia-Pacific region: comparative analysis of the VP1 and VP4 genes. Emerg. Infect. Dis. 9, 461–468.

Chen, B., Sumi, A., Toyoda, S., Hu, Q., Zhou, D., Mise, K., Zhao, J., Kobayashi, N., 2015. Time series analysis of reported cases of hand, foot, and mouth disease from 2010 to 2013 in Wuhan, China. BMC Infect. Dis. 15, 495.

Chen, X., Li, A., Sun, B.F., Yang, Y., Han, Y.N., Yuan, X., Chen, R.X., Wei, W.S., Liu, Y., Gao, C.C., Chen, Y.S., Zhang, M., Ma, X.D., Liu, Z.W., Luo, J.H., Lyu, C., Wang, H.L., Ma, J., Zhao, Y.L., Zhou, F.J., Huang, Y., Xie, D., Yang, Y.G., 2019. 5-methylcytosine promotes pathogenesis of bladder cancer through stabilizing mRNAs. Nat. Cell Biol. 21, 978–990.

Chen, Y., Yang, W., Zhao, Y., Yang, Y., 2021. Dynamic transcriptomic m(5) C and its regulatory role in RNA processing. Wiley Interdiscip Rev RNA 12, e1639.

Courtney, D.G., Kennedy, E.M., Dumm, R.E., Bogerd, H.P., Tsai, K., Heaton, N.S., Cullen, B.R., 2017. Epitranscriptomic enhancement of influenza A virus gene expression and replication. Cell Host Microbe 22, 377–386 e375.

Courtney, D.G., Chalem, A., Bogerd, H.P., Law, B.A., Kennedy, E.M., Holley, C.L., Cullen, B.R., 2019a. Extensive epitranscriptomic methylation of A and C residues on murine leukemia virus transcripts enhances viral gene expression. mBio 10, e01209-19.

Courtney, D.G., Tsai, K., Bogerd, H.P., Kennedy, E.M., Law, B.A., Emery, A., Swanstrom, R., Holley, C.L., Cullen, B.R., 2019b. Epitranscriptomic addition of m(5)C to HIV-1 transcripts regulates viral gene expression. Cell Host Microbe 26, 217–227 e216.

Dawson, M.A., Kouzarides, T., 2012. Cancer epigenetics: from mechanism to therapy. Cell 150, 12–27.

Deng, L., Kumar, J., Rose, R., McIntyre, W., Fabris, D., 2022. Analyzing RNA posttranscriptional modifications to decipher the epitranscriptomic code. Mass Spectrom. Rev., e21798

Ding, S., Liu, H., Liu, L., Ma, L., Chen, Z., Zhu, M., Liu, L., Zhang, X., Hao, H., Zuo, L., Yang, J., Wu, X., Zhou, P., Huang, F., Zhu, F., Guan, W., 2024. Epigenetic addition of m5C to HBV transcripts promotes viral replication and evasion of innate antiviral responses. Cell Death Dis. 15, 39.

Eckwahl, M., Xu, R., Michalkiewicz, J., Zhang, W., Patel, P., Cai, Z., Pan, T., 2020. 5-Methylcytosine RNA modifications promote retrovirus replication in an ALYREF reader protein-dependent manner. J. Virol. 94, e00544-20.

Feng, J., Xu, T., He, M., Li, J., Yao, P., Ma, C., Yang, S., Xu, Z., Yan, K., Chen, X., Wang, H., Liu, J., Zeng, C., Xia, Y., Yan, H., Zhou, L., Chen, Y., 2023. NSUN2-mediated m5C modification of HBV RNA positively regulates HBV replication. PLoS Pathog. 19, e1011808.

Feng, M., Xie, X., Han, G., Zhang, T., Li, Y., Li, Y., Yin, R., Wang, Q., Zhang, T., Wang, P., Hu, J., Cheng, Y., Gao, Z., Wang, J., Chang, J., Cui, M., Gao, K., Chai, J., Liu, W., Guo, C., Li, S., Liu, L., Zhou, F., Chen, J., Zhang, H., 2021. YBX1 is required for maintaining myeloid leukemia cell survival by regulating BCL2 stability in an m6A-dependent manner. Blood 138, 71–85.

Gao, Y., Fang, J., 2021. RNA 5-methylcytosine modification and its emerging role as an epitranscriptomic mark. RNA Biol. 18, 117–127.

Hao, H., Hao, S., Chen, H., Chen, Z., Zhang, Y., Wang, J., Wang, H., Zhang, B., Qiu, J., Deng, F., Guan, W., 2019. N6-methyladenosine modification and METTL3 modulate enterovirus 71 replication. Nucleic Acids Res. 47, 362–374.

Hao, H., Liu, W., Miao, Y., Ma, L., Yu, B., Liu, L., Yang, C., Zhang, K., Chen, Z., Yang, J., Zheng, Z., Zhang, B., Deng, F., Gong, P., Yuan, J., Hu, Z., Guan, W., 2022. N4-acetylcytidine regulates the replication and pathogenicity of enterovirus 71. Nucleic Acids Res. 50, 9339–9354.

Hao, S., Zhang, J., Chen, Z., Xu, H., Wang, H., Guan, W., 2017. Alternative polyadenylation of human bocavirus at its 3' end is regulated by multiple elements and affects capsid expression. J. Virol. 91, e02026-16.

Huang, F., Feng, Y., Peterlin, B.M., Fujinaga, K., 2022. P-TEFb is degraded by Siah1/2 in quiescent cells. Nucleic Acids Res. 50, 5000–5013.

Hussain, S., Sajini, A.A., Blanco, S., Dietmann, S., Lombard, P., Sugimoto, Y., Paramor, M., Gleeson, J.G., Odom, D.T., Ule, J., Frye, M., 2013. NSun2-mediated cytosine-5 methylation of vault noncoding RNA determines its processing into regulatory small RNAs. Cell Rep. 4, 255–261.

Imam, H., Kim, G.W., Siddiqui, A., 2020. Epitranscriptomic(N6-methyladenosine) modification of viral RNA and virus-host interactions. Front. Cell. Infect. Microbiol. 10, 584283.

Kennedy, E.M., Bogerd, H.P., Kornepati, A.V., Kang, D., Ghoshal, D., Marshall, J.B., Poling, B.C., Tsai, K., Gokhale, N.S., Horner, S.M., Cullen, B.R., 2016. Posttranscriptional m(6)A editing of HIV-1 mRNAs enhances viral gene expression. Cell Host Microbe 19, 675–685.
Kim, D., Lee, J.Y., Yang, J.S., Kim, J.W., Kim, V.N., Chang, H., 2020. The architecture of SARS-CoV-2 transcriptome. Cell 181, 914–921 e910.
Li, N., Hui, H., Bray, B., Gonzalez, G.M., Zeller, M., Anderson, K.G., Knight, R., Smith, D., Wang, Y., Carlin, A.F., Rana, T.M., 2021. METTL3 regulates viral m6A RNA modification and host cell innate immune responses during SARS-CoV-2 infection. Cell Rep. 35, 109091.
Lichinchi, G., Gao, S., Saletore, Y., Gonzalez, G.M., Bansal, V., Wang, Y., Mason, C.E., Rana, T.M., 2016. Dynamics of the human and viral m(6)A RNA methylomes during HIV-1 infection of T cells. Nat Microbiol 1, 16011.
Lin, J.Y., Li, M.L., Huang, P.N., Chien, K.Y., Horng, J.T., Shih, S.R., 2008. Heterogeneous nuclear ribonuclear protein K interacts with the enterovirus 71 5' untranslated region and participates in virus replication. J. Gen. Virol. 89, 2540–2549.
Liu, Y., Zheng, Z., Shu, B., Meng, J., Zhang, Y., Zheng, C., Ke, X., Gong, P., Hu, Q., Wang, H., 2016. SUMO modification stabilizes enterovirus 71 polymerase 3D to facilitate viral replication. J. Virol. 90, 10472–10485.
Lopata, A., Kniss, A., Lohr, F., Rogov, V.V., Dotsch, V., 2020. Ubiquitination in the ERAD process. Int. J. Mol. Sci. 21, 5369.
Lv, X., Liu, X., Zhao, M., Wu, H., Zhang, W., Lu, Q., Chen, X., 2021. RNA methylation in systemic lupus erythematosus. Front. Cell Dev. Biol. 9, 696559.
Majumder, K., Morales, A.J., 2021. Utilization of host cell chromosome conformation by viral pathogens: knowing when to hold and when to fold. Front. Immunol. 12, 633762.
Meyer, K.D., 2019. m(6)A-mediated translation regulation. Biochim Biophys Acta Gene Regul Mech 1862, 301–309.
Motorin, Y., Helm, M., 2011. RNA nucleotide methylation. Wiley Interdiscip Rev RNA 2, 611–631.
Pathinayake, P.S., Hsu, A.C., Wark, P.A., 2015. Innate immunity and immune evasion by enterovirus 71. Viruses 7, 6613–6630.
Reid, R., Greene, P.J., Santi, D.V., 1999. Exposition of a family of RNA m(5)C methyltransferases from searching genomic and proteomic sequences. Nucleic Acids Res. 27, 3138–3145.
Roundtree, I.A., Evans, M.E., Pan, T., He, C., 2017. Dynamic RNA modifications in gene expression regulation. Cell 169, 1187–1200.
Schumann, U., Zhang, H.N., Sibbritt, T., Pan, A., Horvath, A., Gross, S., Clark, S.J., Yang, L., Preiss, T., 2020. Multiple links between 5-methylcytosine content of mRNA and translation. BMC Biol. 18, 40.
Shi, H., Wei, J., He, C., 2019. Where, when, and how: context-dependent functions of RNA methylation writers, readers, and erasers. Mol Cell. 74, 640–650.
Song, P., Tayier, S., Cai, Z., Jia, G., 2021. RNA methylation in mammalian development and cancer. Cell Biol. Toxicol. 37, 811–831.
Srinivas, K.P., Depledge, D.P., Abebe, J.S., Rice, S.A., Mohr, I., Wilson, A.C., 2021. Widespread remodeling of the m(6)A RNA-modification landscape by a viral regulator of RNA processing and export. Proc Natl Acad Sci U S A 118, e2104805118.
Sweeney, T.R., Abaeva, I.S., Pestova, T.V., Hellen, C.U., 2014. The mechanism of translation initiation on Type 1 picornavirus IRESs. EMBO J. 33, 76–92.
Tsai, K., Jaguva Vasudevan, A.A., Martinez Campos, C., Emery, A., Swanstrom, R., Cullen, B.R., 2020. Acetylation of cytidine residues boosts HIV-1 gene expression by increasing viral RNA stability. Cell Host Microbe 28, 306–312.e306.
Wang, T., Kong, S., Tao, M., Ju, S., 2020. The potential role of RNA N6-methyladenosine in Cancer progression. Mol. Cancer 19, 88.
Wiener, D., Schwartz, S., 2021. The epitranscriptome beyond m(6)A. Nat. Rev. Genet. 22, 119–131.
Wu, L., Candille, S.I., Choi, Y., Xie, D., Jiang, L., Li-Pook-Than, J., Tang, H., Snyder, M., 2013. Variation and genetic control of protein abundance in humans. Nature 499, 79–82.
Xiao, X., Qi, J., Lei, X., Wang, J., 2019. Interactions between enteroviruses and the inflammasome: new insights into viral pathogenesis. Front. Microbiol. 10, 321.
Yang, X., Yang, Y., Sun, B.F., Chen, Y.S., Xu, J.W., Lai, W.Y., Li, A., Wang, X., Bhattarai, D.P., Xiao, W., Sun, H.Y., Zhu, Q., Ma, H.L., Adhikari, S., Sun, M., Hao, Y.J., Zhang, B., Huang, C.M., Huang, N., Jiang, G.B., Zhao, Y.L., Wang, H.L., Sun, Y.P., Yang, Y.G., 2017. 5-methylcytosine promotes mRNA export - NSUN2 as the methyltransferase and ALYREF as an m(5)C reader. Cell Res. 27, 606–625.
Yang, Y., Wang, L., Han, X., Yang, W.L., Zhang, M., Ma, H.L., Sun, B.F., Li, A., Xia, J., Chen, J., Heng, J., Wu, B., Chen, Y.S., Xu, J.W., Yang, X., Yao, H., Sun, J., Lyu, C., Wang, H.L., Huang, Y., Sun, Y.P., Zhao, Y.L., Meng, A., Ma, J., Liu, F., Yang, Y.G., 2019. RNA 5-methylcytosine facilitates the maternal-to-zygotic transition by preventing maternal mRNA decay. Mol Cell 75, 1188–1202.e1111.
Zhang, X., Hao, H., Ma, L., Zhang, Y., Hu, X., Chen, Z., Liu, D., Yuan, J., Hu, Z., Guan, W., 2021. Methyltransferase-like 3 modulates severe acute respiratory syndrome coronavirus-2 RNA N6-methyladenosine modification and replication. mBio 12, e0106721.
Zhao, Y., Shi, Y., Shen, H., Xie, W., 2020. m(6)A-binding proteins: the emerging crucial performers in epigenetics. J. Hematol. Oncol. 13, 35.